Assimilating MODIS aerosol optical depth using WRF/Chem and GSI: Application to a Chinese dust storm

Zhiquan Liu[1], Quanhua Liu[2], Hui-Chuan Lin[1], Craig S. Schwartz[1] and Yen-Huei Lee[1]

[1]National Center for Atmospheric Research, Boulder, CO, USA

[2]Joint Center for Satellite Data Assimilation, Camp Springs, MD, USA

Abstract

Assimilation of the Moderate Resolution Imaging Spectroradiometer (MODIS) total aerosol optical depth (AOD) retrieval products (at 550 nm wavelength) from both Terra and Aqua satellites have been developed within the National Centers for Environmental Prediction (NCEP) Gridpoint Statistical Interpolation (GSI) three-dimensional variational (3DVAR) data assimilation system. This newly developed algorithm allows, in a one-step procedure, the analysis of 3D mass concentration of 14 aerosol variables from the Goddard Chemistry Aerosol Radiation and Transport (GOCART) module. The Community Radiative Transfer Model (CRTM) was extended to calculate AOD using GOCART aerosol variables as input. Both the AOD forward model and corresponding Jacobian model were developed within the CRTM and used in the 3DVAR minimization algorithm to compute the AOD cost function and its gradient with respect to 3D aerosol mass concentration. The impact of MODIS AOD data assimilation was demonstrated by application to a dust storm from 17 to 24 March 2010 over East Asia. The aerosol analyses initialized Weather Research and Forecasting/Chemistry (WRF/Chem) model forecasts. Results indicate that assimilating MODIS AOD substantially improves aerosol analyses and subsequent forecasts when compared to independent AOD observations from the AErosol RObotic NETwork (AERONET) and Cloud-Aerosol Lidar with Orthogonal Polarization (CALIOP) instrument. The newly developed AOD data assimilation system can serve as a tool to improve simulations of dust storms and general air quality analyses and forecasts.

1. Introduction

Aerosol data assimilation has received attention during the past decade. For example, *Collins et al*. [2001] introduced assimilating AVHRR AOD in a three-dimensional (3D) chemical transport model while studying the INDOEX (Indian Ocean Experiment) aerosols. They used an optimal interpolation (OI) technique initially developed for meteorological applications. Since then, several other studies have assimilated satellite-derived aerosol products in global and regional chemical transport models using similar OI techniques [*Yu et al*., 2003; *Generoso et al*., 2007; *Adhikary et al*., 2008]. Additionally, *Zhang et al*. [2008] adopted a two-dimensional variational (2DVAR) approach to assimilate MODIS gridded level 3 AOD products over the global ocean with the Naval Research Laboratory (NRL) Aerosol Analysis and Prediction System (NAAPS). Furthermore, *Niu et al*. [2007] used a 3DVAR method to assimilate dust loading retrieved from Chinese geostationary satellite FY-2C into the Chinese Unified Atmospheric Chemistry Environment–Dust (CUACE/Dust) forecast system. More recently, the European Centre for Medium-Range Weather Forecasts (ECMWF) extended its

four-dimensional variational (4DVAR) meteorological assimilation system to include an aerosol component [*Benedetti et al*., 2009]. *Benedetti et al.* [2009] adopted the total aerosol mixing ratio as a control variable and made some assumptions to partition the total aerosol mass into mass concentration of individual species. Their application to a 2-year (2003, 2004) reanalysis using MODIS AOD data showed the analyses were skillful at fitting the observations and improving AOD forecasts.

We note that most of the aerosol DA methods (OI, 2DVAR, and 3DVAR) mentioned above used a two-step process: 2D AOD or 3D DM40 [dust particle matter with diameter less than 40 μm; *Niu et al*., 2007] is first analyzed from aerosol observations and then partitioned using a post-processing procedure into 3D mass concentrations of different aerosol species, making assumptions regarding vertical distribution and relative ratio of individual species' mass to total aerosol mass. In this study, we develop a single-step aerosol DA capability within the National Centers for Environmental Prediction (NCEP) operational Gridpoint Statistical Interpolation (GSI) 3DVAR meteorological DA system coupled to the Weather Research and Forecasting/Chemistry (WRF/Chem) model [*Grell et al*., 2005]. We then use this system to assimilate MODIS AOD data while modeling a dust storm that occurred in March 2010 over East Asia. Different from previous studies, the newly developed 3DVAR aerosol DA system uses individual aerosol species of the WRF/Chem built-in GOCART module as "control variables." Therefore, 3D mass concentrations of the aerosol species are analyzed in a one-step minimization procedure, obviating the need for a second-step post-processing required by previous studies. To the best of our knowledge, this is the first attempt to use individual aerosol species as analysis variables in a truly 3DVAR DA system.

The next section briefly describes the WRF/Chem model and built-in GOCART aerosol module. Section 3 presents the methodology of aerosol DA, including a description of the aerosol background error covariance (BEC) statistics, MODIS AOD observations, and CRTM-AOD observation operator. The experimental design and impact of AOD assimilation applied to a dust storm are described in section 4 before concluding in section 5.

2. Methodology of aerosol data assimilation

To find a best estimate of the model state **x** in the sense of minimum analysis error variance, a 3DVAR algorithm is to minimize a cost function (J) that measures the distance of the state vector to the background and observations, given by

$$J(\mathbf{x}) = \frac{1}{2}(\mathbf{x}-\mathbf{x_b})^{\mathrm{T}}\mathbf{B}^{-1}(\mathbf{x}-\mathbf{x_b}) + \frac{1}{2}[H(\mathbf{x})-\mathbf{y}]^{\mathrm{T}}\mathbf{R}^{-1}[H(\mathbf{x})-\mathbf{y}], \qquad (1)$$

where **B** and **R** are the background and observation error covariance matrices of dimensions m×m and p×p, respectively. **B** and **R** determine the relative contributions of the background and observation terms to the final analysis. As **x** and **y** are column vectors, ***J(x)*** is simply a scalar.

For our implementation of AOD DA, the 3D mass concentrations of the 14 WRF/Chem GOCART aerosol species within the entire domain and at all model levels comprised the analysis variables (or "control variables") in the GSI 3DVAR minimization procedure. Therefore, it was necessary to calculate BEC statistics for each aerosol variable. We accomplished this task by using the "NMC" method [*Parrish and Derber*, 1992], which calculates BECs by taking differences between forecasts of different lengths valid at common times. Differences of 24- and 12-hr WRF/Chem forecasts of the aerosol species valid at the same time for 62 pairs valid at either 0000 and 1200 UTC over the whole month of March 2010 were used to compute the aerosol BECs. ICs and LBCs for each forecast came from the NCAR global

CAM-Chem model. In this first implementation, no cross-correlation between different aerosol variables was considered due to the incapability of the current GSI 3DVAR to directly model the cross-correlation in the B-matrix. Standard deviations and horizontal and vertical length scales for each aerosol variable were calculated using the method described by *Wu et al*. [2002]. The domain average standard deviations at each model level are shown for all 14 species in Figure 1. Standard deviations varied substantially across the species, spanning several orders of magnitude, which corresponded to different magnitude of the species' mass concentrations. The values of the horizontal length scale (not shown) were comparable for all the species, generally spanning ~1.5-2.5 times the grid spacing (27km).

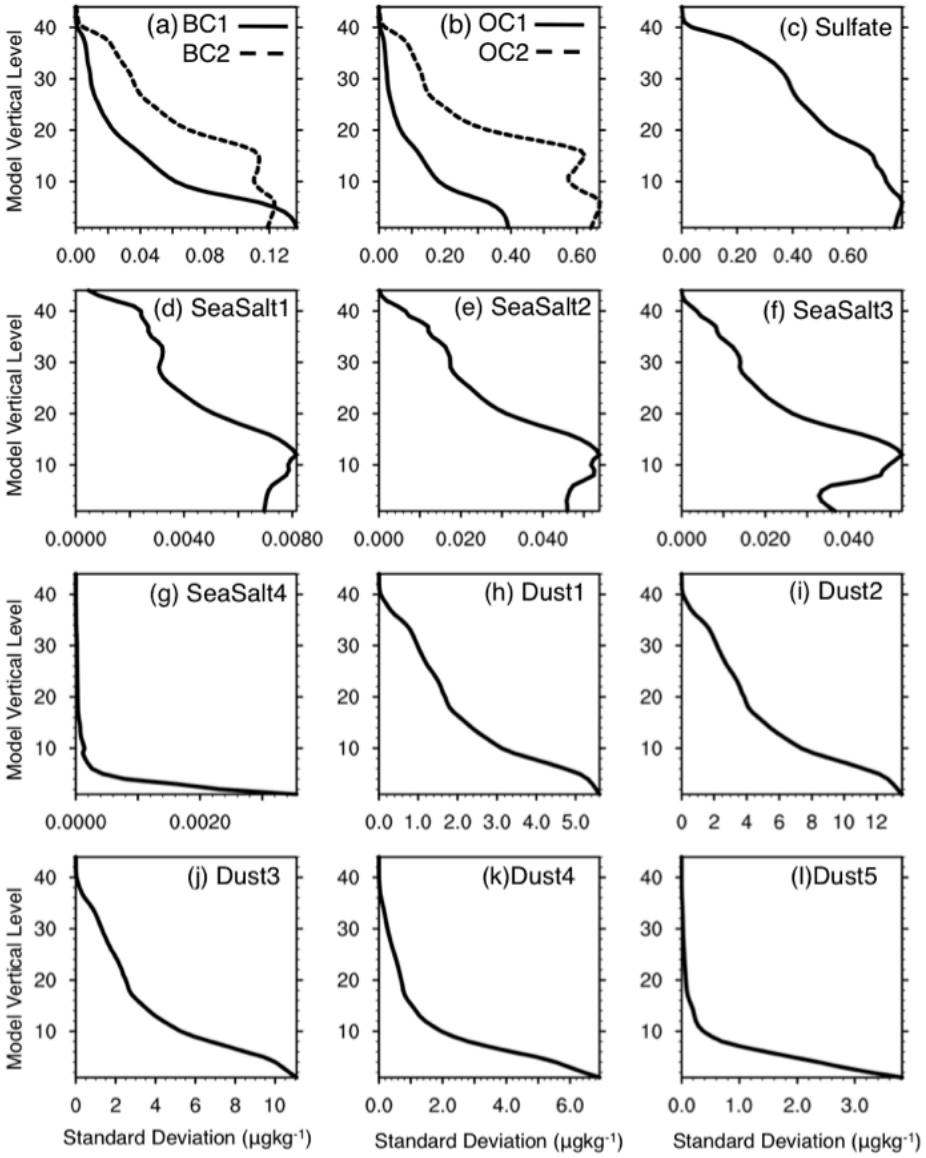

Figure 1. Domain-averaged background error standard deviation (μgkg^{-1}) for each model level (*y*-axis) for 14 GOCART aerosol species.

We used the most recent release (collection 051) of level 2 total AOD retrievals from both Terra and Aqua. To maximize the observation coverage within ±3-hr data assimilation time window, we used AOD retrievals over land and sea derived from the dark target product [*Remer et al*., 2005] and "deep-blue" product over bright land surface [*Hsu et al*., 2004]. The dark target ocean and land AOD products were available from both Terra and Aqua, but deep-blue retrievals were only available from Aqua. Only the optical depth at 0.55 μm was assimilated in this study. In our domain, MODIS AOD products provided coverage only at 0000 and 0600 UTC (day time) with generally only Terra at 0000 UTC, and both Terra and Aqua at 0600 UTC with more coverage. Figure 2 shows the AOD coverage within a ±3-hr time window centered at 0600 UTC on 21 March 2010. Most data were distributed in southern and eastern parts of the domain and the deep-blue product from Aqua had sparse coverage over Mongolia and northwestern China, typical source regions of Chinese dust storms.

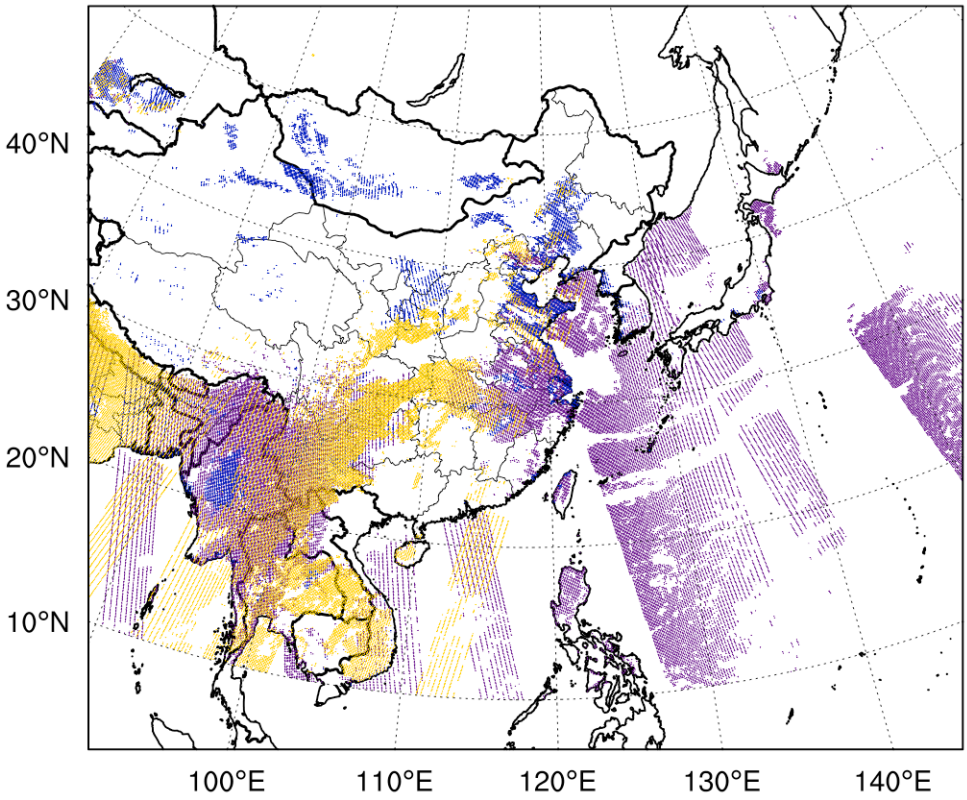

Figure 2. MODIS AOD coverage from the Aqua and Terra satellites at 0600 UTC 21 March 2010. Purple: dark-surface retrievals from Aqua; gold: dark surface Terra; blue: deep-blue produced from Aqua.

The AOD observation operator is based upon the community radiative transfer model [CRTM; *Han et al*., 2006] developed at the United States Joint Center for Satellite Data Assimilation (JCSDA). The CRTM was primarily designed for computing satellite radiances and is used in GSI for directly assimilating radiances from infrared and microwave sensors. We extended the CRTM to compute MODIS AOD using only aerosol profiles as input. This newly developed CRTM-AOD module was incorporated into the GSI system.

3. Experimental design

A dust storm that started in Mongolia blasted Beijing on 20 March 2010 and covered large areas of China in the following days. Several countries in East Asia were affected. Hong Kong,

Taiwan, Japan, and South Korea recorded extremely poor visibility and air quality was hazardous to human health. The dust was lofted by strong winds accompanying a cold front that crossed China on 20 March. The winds passed over regions of Mongolia and northwest China that had been suffering from an extended drought.

Two parallel experiments were designed to evaluate the impact of MODIS AOD DA on analyses and forecasts of aerosols over eastern Asia. One experiment served as the control and did not employ any DA, while AOD DA was implemented in the other. Each experiment initialized a new WRF/Chem forecast every 6-hrs between 0000 UTC 17 March and 0000 UTC 24 March 2010 (inclusive). All forecasts were integrated for 6-hrs and hourly model output was archived. Every initialization, both experiments' meteorological fields were updated by interpolating GFS analyses onto the computational domain. Gaseous chemical variables were initialized from the previous cycle's 6-hr forecast, except for the first forecast (0000 UTC 17 March), when gaseous and aerosol ICs came from NCAR global CAM-Chem model output.

The two experiments only differed in that 3DVAR DA updated the profiles of GOCART aerosol species in one experiment but not the other, permitting a clear isolation of the impact of cyclic AOD DA. Note that MODIS AOD data were only present during the day (0000 and 0600 UTC), and therefore, the aerosol fields valid at 0000 UTC should be considered as 18-hr forecasts initialized at 0600 UTC the previous day, since no AOD observations were present at 1200 or 1800 UTC to update aerosol fields. However, meteorological fields were still updated from GFS analyses at 1200 and 1800 UTC.

The WRF/Chem model was run over a computation domain (Figure 2) with 27-km horizontal grid spacing. There were 261 west-east and 222 south-north horizontal grid points and 45 vertical levels. The model-top was 50 hPa. The following physical parameterizations were included: the WRF single-moment 5-class (WSM5) microphysics scheme; the Rapid Radiative Transfer Model (RRTM) longwave and Goddard shortwave radiation schemes; the Mellor-Yamada-Janjic (MYJ) boundary layer scheme; the Noah land surface model; and Grell-3D cumulus parameterization. Lateral boundary conditions (LBCs) for meteorological fields were provided by the NCEP Global Forecast System (GFS). Aerosol and chemical initial conditions (ICs) (at the beginning of the simulation period) and LBCs came from the National Center for Atmospheric Research (NCAR) global CAM-Chem model. The online calculation of biogenic emissions using the U.S. Geological Survey (USGS) landuse classification was adopted as by *Simpson et al*. [1995]. Two anthropogenic emissions inventories were used: gaseous chemistry emissions from the global (0.5° X 0.5°) RETRO (REanalysis of the TROpospheric chemical composition over the past 40 years) inventory (http://retro.enes.org/) and gridded 0.5° X 0.5° aerosol emissions from an Asia emissions inventory [*Streets et al*., 2003]. The dust emission flux is computed as a function of probability source function and surface wind speed [*Ginoux et al.*, 2001]. Similar to dust uplifting, sea salt emissions from the ocean are highly dependent on the surface wind speed and calculated as a function of wind speed at 10 m and sea salt particle radius [*Chin et al*., 2002].

4. Results

4.1 Comparison to AERONET AOD

Figure 3 depicts the hourly time series of AOD at 500 nm for the whole experimental period (0000 UTC 17 through 0600 UTC 24 March) at six AERONET sites in the domain. Among those sites, Nanjing, Jhongli of Taiwan, and Hong Kong were affected by the dust storm. The analyzed AOD values after DA are shown only at 0000 and 0600 UTC, when MODIS AOD data

were present. Otherwise, hourly model *forecast* output is displayed. The NoDA experiment (green lines) produced AOD values far below AERONET observations (red lines), but assimilating MODIS AOD (blue lines) yielded AOD values much closer to AERONET observations, although to different extents among the sites and dates. The peak AOD values in Nanjing around 0600 UTC 21 March (Figure 3a), during the dust storm, were simulated quite well by the DA experiment. AOD DA's capability to capture the extreme event around 0600 UTC 21 March was also evident in Ubon Ratchathani (Figure 3e). The decease of AOD values beginning 22 March in Dongsha Island was also well depicted in the DA experiment. At early times of the simulation period, AOD values at some sites (e.g., Dongsha Island and Bangkok) were underestimated even with AOD DA, likely due to no coverage of MODIS AOD data.

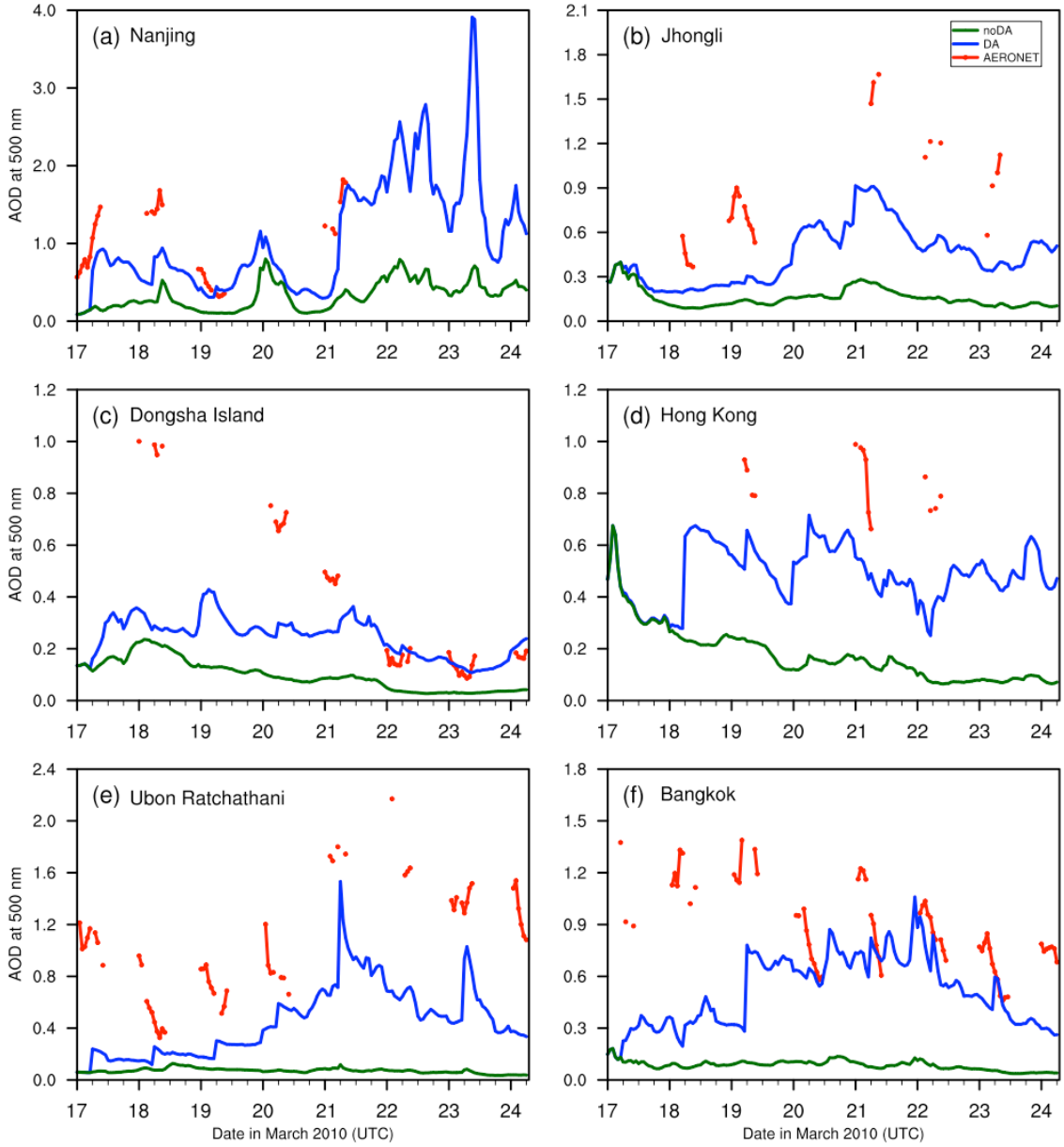

Figure 3. Hourly time series of total AOD at 500 nm from 0000 UTC 17 March to 0600 UTC 24 March, at 6 AERONET sites. Model output is hourly. Red line denotes the AERONET observations, and blue and green curves represent the DA and NoDA experiments, respectively.

Figure 4 shows AOD verification at four wavelengths (1640, 1020, 870, and 675 nm) at an AERONET site in Kathmandu, the capital and largest city of Nepal. This site was unaffected by the dust storm and typical air-pollution dominated the AOD. The NoDA experiment severely underestimated AOD compared to the AERONET observations, likely revealing the underestimated emissions from the "Streets" 2006 Asia emissions inventory used for emissions in our study. However, assimilation of current data provides a method to overcome shortcomings of "climatological" emissions. The AOD values from the DA experiment (blue line) agree more closely with AERONET observations. The minimum AOD values around 0600 UTC (local noon) were captured, particularly for longer wavelengths (1640 and 1020 nm). Kathmandu is one of the most polluted cities in Asia, partly due to high year-round traffic volume of fuel-inefficient vehicles. The diurnal variation of AOD in the AERONET observations, and replicated by the DA experiment, likely reflects changes in traffic from the morning to evening.

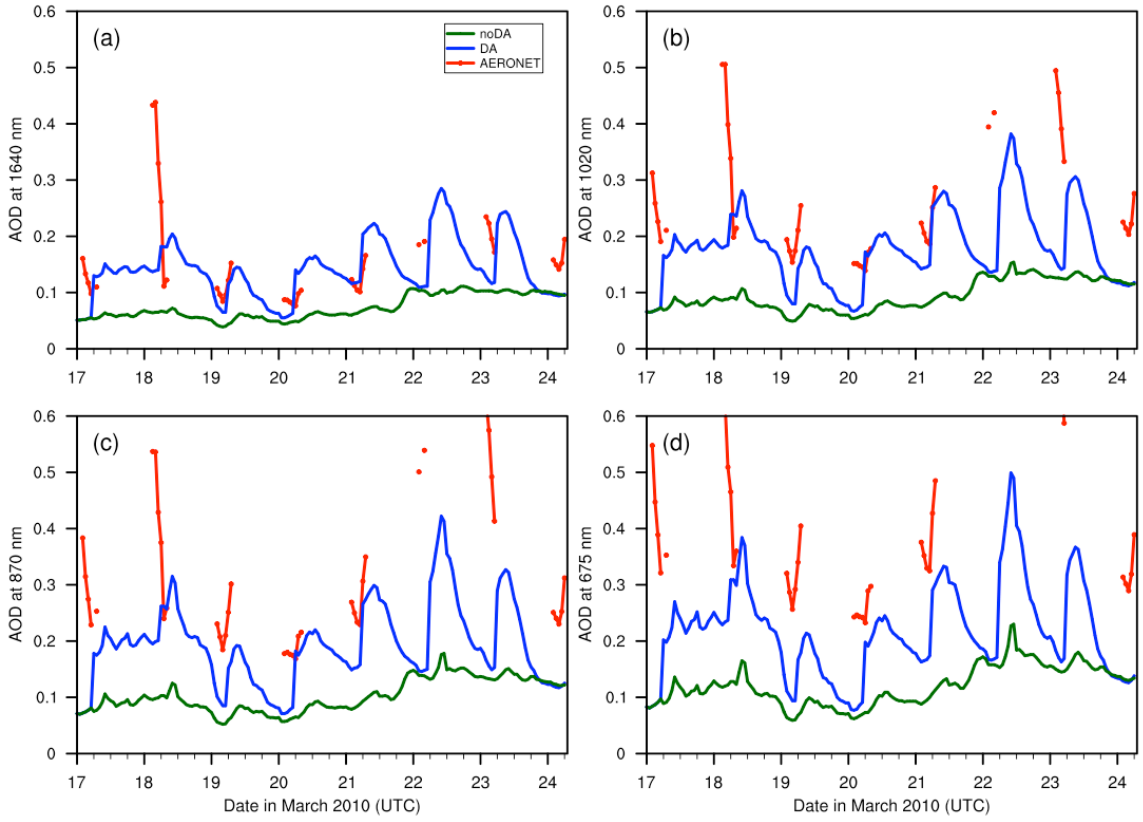

Figure 4. As in Figure 3, but for AOD validation at four wavelengths (1640, 1020, 870, and 675 nm) at the Kathmandu AERONET site.

4.2 Comparison to CALIOP AOD

CALIPSO flies in a near-nadir view so that CALIOP footprints nominally fall on the satellite ground track. The CALIOP AOD product is provided at 5 km (60 m) horizontal (vertical) resolution and was averaged to match the model horizontal resolution (27 km) and vertical grid before comparing to the model output. Figure 5 shows the results at 532 nm of CALIOP transects around 1700 UTC 19 March (Figure 5a-c) and 2000 UTC 20 March (Fig. 5d-f). The AOD model output is essentially from an 11-hr (14-hr) forecast for the case on the 19th (20th). The model times differ from those of the CALIOP observations by ~40 min (~15 min) for the

path on 19 March (20 March). Larger AOD values were produced by the DA experiment on both dates, while the patterns were similar for both experiments. As shown in Figures 5c,f, the DA experiment agreed more with CALIOP than the NoDA experiment for both paths. The improvement through DA is particularly evident in the southeast part of the domain on 20 March. We note that CALIOP AOD measurements were retrieved only from cloud-free layers, whereas the model AOD was obtained from integration over all model layers, regardless of whether clouds were present. This difference may explain some of the discrepancies between the model-predicted and CALIOP AODs in Figure 5.

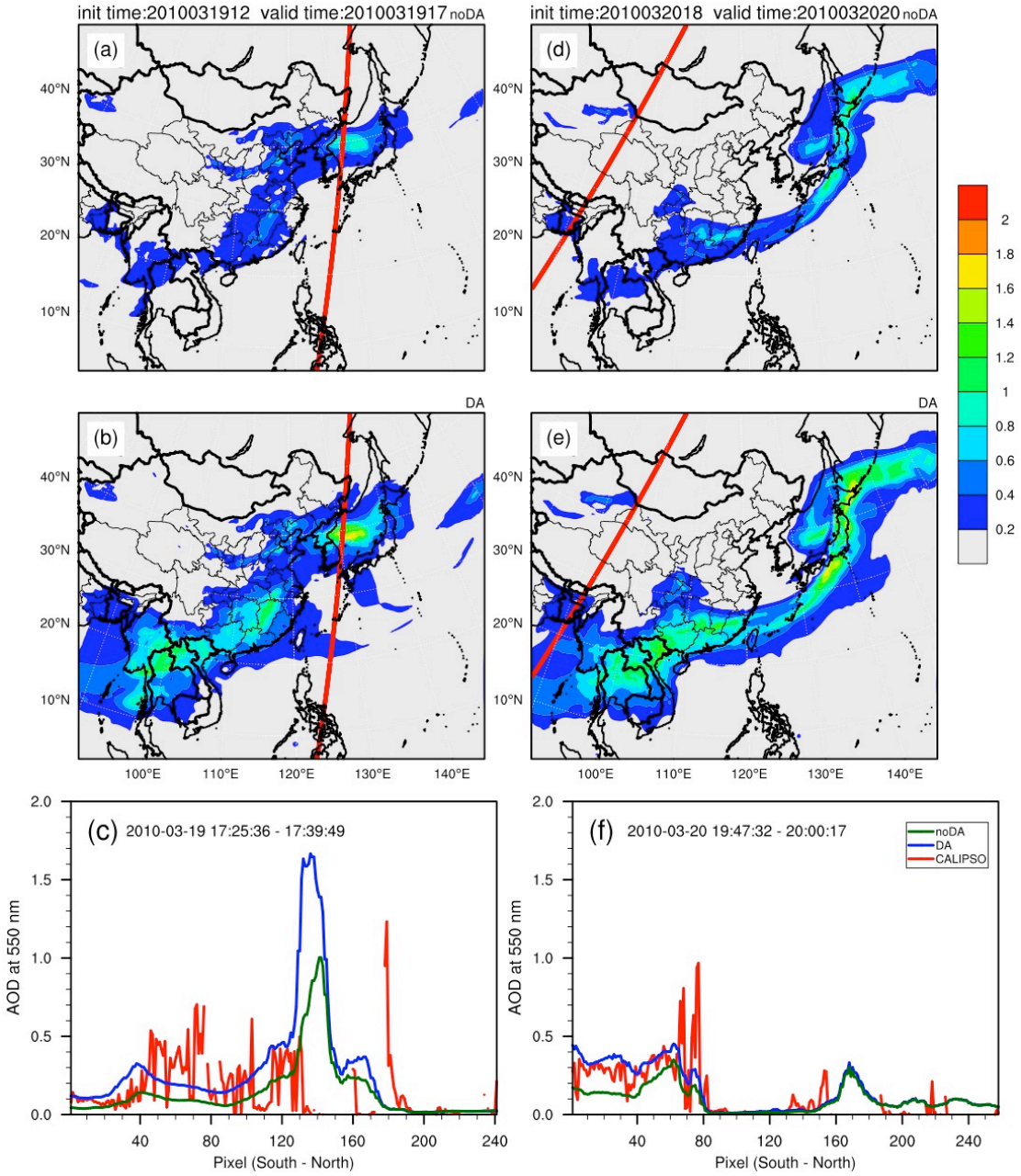

Figure 5. Model 550 nm AOD forecasts from (a, d) the NoDA experiment and (b, e) the DA experiment overlaid with CALIPSO path, and (c, f) 532 nm AOD values along the CALIPSO path from CALIOP observations (red), and 550 nm model AOD output from DA (blue) and NoDA (green) experiment. Left panels (a)-(c) are valid around 1700 UTC 19 March and right panels (d)-(f) around 2000 UTC 20 March.

The vertical distributions of 532 nm CALIOP AOD and 550 nm model AOD output corresponding to Figure 5f are given in Figure 6. Both experiments well simulated the AOD vertical distributions within the 1 km – 2 km layer in the southern part of the CALIPSO path. Clearly, the larger AOD values from the DA experiment agreed more closely with the CALIOP observations.

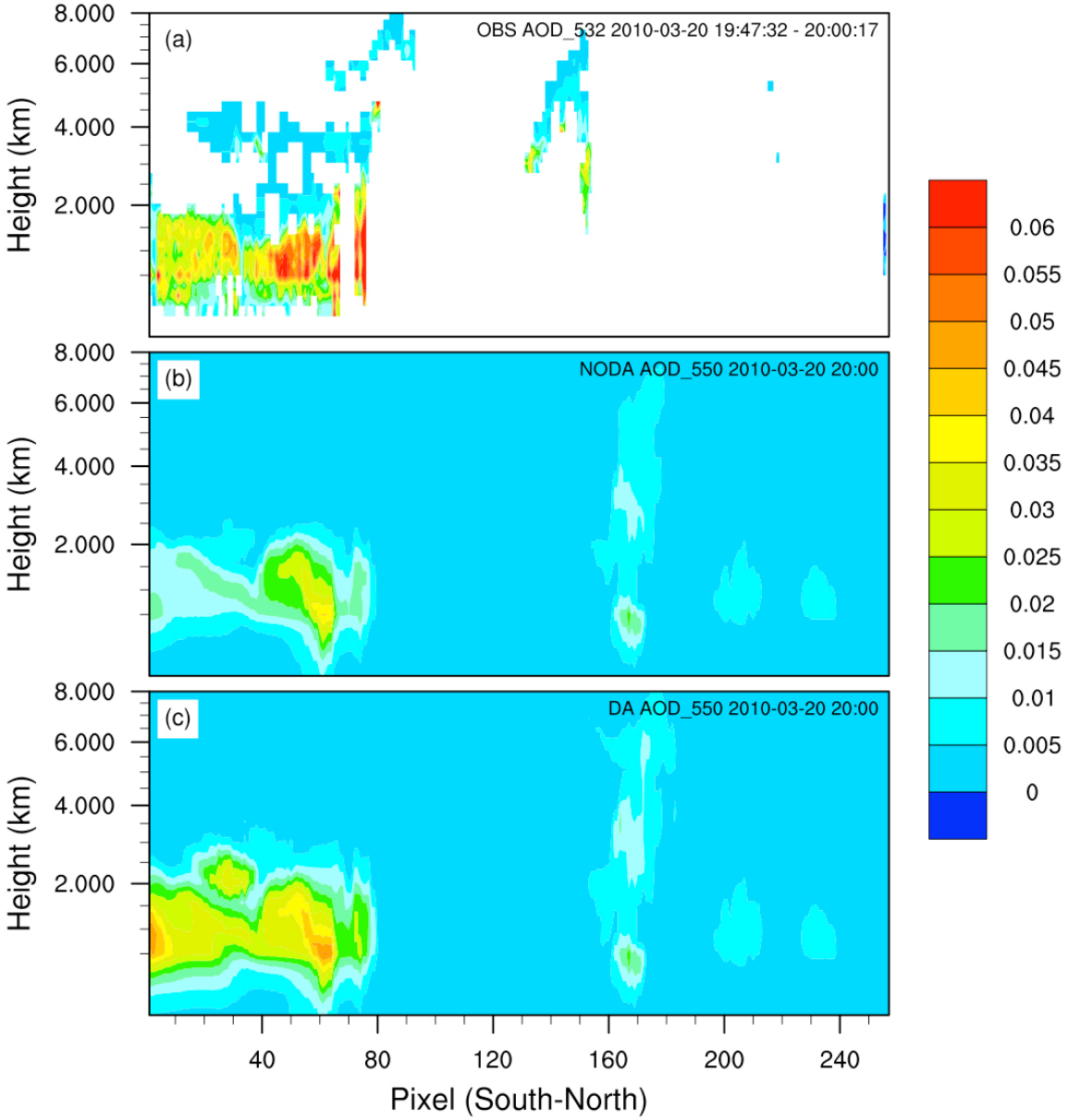

Figure 6. Similar to Figure 5f, but corresponding vertical distributions of (a) 532 nm CALIOP AOD and 550 nm AOD from (b) NoDA and (c) DA experiments around 2000 UTC 20 March.

5. Conclusions

The GSI 3DVAR DA system was expanded to assimilate MODIS AOD observations using 3D mass concentrations of 14 GOCART aerosol species as analysis variables. The CRTM was extended to serve as the AOD observation operator (both forward operator and Jacobian) and computed model-simulated AOD from the aerosol profiles. Some developments, such as adding

aerosol analysis variables in the GSI and the corresponding background error statistics, are applicable to the assimilation of any aerosol related observations. Our one-step procedure did not impose any constraints or assumptions about the relative contribution of each species' mass concentration to the total aerosol mass concentration, in contrast to traditional two-step approaches. Thus, AOD observations could directly impact the analysis profiles of individual species.

The impact of the newly developed AOD DA system was demonstrated by application to a dust storm that occurred in March 2010 over eastern Asia. Aerosol analyses and forecasts were validated against AOD observations from independent data sources (AERONET and CALIOP). The WRF/Chem model simulation without AOD DA severely underestimated the dust storm intensity, and, thus, the corresponding AOD values. However, AOD DA reduced the model low bias for aerosol forecasts by inflating the initial 3D aerosol mass concentrations. The results indicate that our one-step 3DVAR method of assimilating MODIS AOD permits concentrations of individual aerosol species to change while maintaining similar vertical structures before and after DA.

The AOD DA capability we developed here is just the first step toward a more comprehensive aerosol DA system. It is fairly straightforward to expand the system to assimilate additional aerosol-related observations (e.g., surface measurements of particle matter, multi-spectral and multi-angle AOD retrievals from different satellite instruments, vertical extinction profiles from ground-based and space-borne Lidar),and, thus, refine vertical structures of individual species and better quantify each species' contribution to the total aerosol mass. New aerosol variables can be added to the state vector and the corresponding BECs determined easily. Moreover, our 3DVAR system can simultaneously assimilate MODIS AOD and meteorological observations typically used in GSI. This capability will be tested in future work to study the interaction between meteorological and aerosol assimilation.

Lastly, it should be recognized that DA is a supplemental tool and not the only way of improving aerosol analyses and forecasts. Chemical and aerosol models themselves should continue to be improved through more accurate estimations of emissions and better modeling of various physical and chemical processes.

Acknowledgements

We are grateful to the Air Force Weather Agency for funding this work. AERONET Principal Investigators are also thanked for making their data available. NCAR is sponsored by the National Science Foundation.

References

Adhikary, B., S. Kulkarni, A. D'allura, Y. Tang, T. Chai,L. R. Leung,Y. Qian, C. E. Chung,V. Ramanathan, and G. R. Carmichael (2008), A regional scale chemical transport modeling of Asian aerosols with data assimilation of AOD observations using optimal interpolation technique, *Atmos. Env.,* 42(37), 8600-8615.

Benedetti, A., et al. (2009), Aerosol analysis and forecast in the European Centre for Medium-Range Weather Forecasts Integrated Forecast System: 2. Data assimilation, *J. Geophys. Res.*, 114, D13205, doi:10.1029/2008JD011115.

Chin, M., P. Ginoux, S. Kinne, O. Torres, B. N. Holben, B. N. Duncan, R. V. Martin, J. A. Logan, and A. Higurashi (2002), Tropospheric aerosol optical thickness from the

GOCART model and comparisons with satellite and sun photometer measurements, *J. Atmos. Sci.*, **59,** 461–483.

Collins, W. D., P. J. Rasch, B. E. Eaton, B. V. Khattatov, and J.-F. Lamarque (2001), Simulating aerosols using a chemical transport model with assim- ilation of satellite aerosol retrievals: Methodology for INDOEX, J. Geo- phys. Res., 106, 7313–7336.

Generoso, S., F.-M. Bréon, F. Chevallier, Y. Balkanski, M. Schulz, and I. Bey (2007), Assimilation of POLDER aerosol optical thickiness into the LMDz–INCA model: Implications for the Arctic aerosol burden, *J. Geophys. Res*., 112, D02311, doi:10.1029/2005JD006954.

Ginoux, P., M. Chin, I. Tegen, J. Prospero, B. Holben, O. Dubovik, and S-J. Lin (2001), Sources and distributions of dust aerosols simulated with the GOCART model, *J. Geophys. Res*, **106,** 20225–20273.

Grell, G. A., S. E. Peckham, R. Schmitz, S. A. McKeen, G. Frost, W. C. Skamarock and B. Eder (2005), Fully coupled "online" chemistry within the WRF model, *Atmos. Environ.,* **39,** 6957–6975.

Han, Y., P. van Delst, Q. Liu, F. Weng, B. Yan, R. Treadon, and J. Derber (2006), JCSDA Community Radiative Transfer Model (CRTM)—Version 1. NOAA Tech. Rep. NESDIS 122, 33 pp.

Hsu, N.C., S.-C. Tsay, M.D. King, and J.R. Herman (2006), Deep Blue retrieval of Asia aerosol properties during ACE-Asia, *IEEE Trans. Geosci. Remote Sens*., **44**, 3180-3195.

Niu, T., S. L. Gong, G.F Zhu, H.L. Liu, X.Q. Hu, C.H. Zhou, Y.Q. Wang, and X.Y. Zhang (2007), Data assimilation of dust aerosol observations for CUACE/dust forecasting system, *Atmospheric Chemistry and Physics Discussion*, 7, 8309–8332.

Parrish, D. F., and J. C. Derber (1992), The National Meteorological Center's spectral statistical interpolation analysis system, *Mon. Wea. Rev.*, **120,** 1747–1763.

Remer, L. A., and Coauthors, 2005: The MODIS Aerosol Algorithm, Products, and Validation. *J. Atmos. Sci.*, **62**, 947–973. doi: 10.1175/JAS3385.1

Simpson, D., A. Guenther, C. N. Hewitt, and R. Steinbrecher (1995), Biogenic emissions in Europe. 1. Estimates and uncertainties. *J. Geophys. Res.,* **100D,** 22875–22890.

Streets, D.G., T.C. Bond, G.R. Carmichael, S.D. Fernandes, Q. Fu, Z. Klimont, S.M. Nelson, N.Y. Tsai, M.Q. Wang, J-H. Woo, and K.F. Yarber (2003), An inventory of gaseous and primary aerosol emissions in Asia in the year 2000, *J. Geophys. Res*, **108**, D21, doi:10.1029/2002JD003093.

Wesley, M. L. (1989), Parameterization of surface resistance to gaseous dry deposition in regional-scale numerical models. *Atmos. Environ*., 23, 1293–1304.

Wu, W.-S., D. F. Parrish, and R. J. Purser (2002), Three-dimensional variational analysis with spatially inhomogeneous covariances, *Mon. Wea. Rev*., 130, 2905–2916.

Yu, H., R.E. Dickinson, M. Chin, Y.J. Kaufman, B. Geogdzhayev, M.I. Mishchenko (2003), Annual cycle of global distributions of aerosol optical depth from integration of MODIS retrievals and GOCART model simulations, *J. Geophys Res*., 108(D3), 4128, doi:10.1029/2002JD002717.

Zhang, J. and J. S. Reid, D. Westphal, N. Baker, and E. Hyer (2008), A System for Operational Aerosol Optical Depth Data Assimilation over Global Oceans, *J. Geophys. Res.,* 113, D10208, doi:10.1029/2007JD009065.